



Electrospun colourimetric sensors for detecting volatile amines

Sebastian Ulrich^{a,1}, Sara Oliveira Moura^{a,b,c,1}, Yvonne Diaz^d, Michèle Clerc^a, Anne Géraldine Guex^{a,e}, Javier Read de Alaniz^d, Albino Martins^{b,c}, Nuno M. Neves^{b,c}, Markus Rottmar^e, René M. Rossi^a, Giuseppino Fortunato^a, Luciano F. Boesel^{a,*}

^a Empa, Swiss Federal Laboratories for Materials Science and Technology, Laboratory for Biomimetic Membranes and Textiles, Lerchenfeldstrasse 5, 9014 St. Gallen, Switzerland

^b 3B's Research Group, I3Bs – Research Institute on Biomaterials, Biodegradables and Biomimetics of University of Minho, Headquarters of the European Institute of Excellence on Tissue Engineering and Regenerative Medicine, AvePark - Parque de Ciência e Tecnologia, Zona Industrial da Gandra, 4805-017, Barco, Guimarães, Portugal

^c ICVS/3B's - PT Government Associate Laboratory, Braga/Guimarães, Portugal

^d Department of Chemistry and Biochemistry, University of California, Santa Barbara, CA, 93106, United States

^e Empa, Swiss Federal Laboratories for Materials Science and Technology, Biointerfaces, Lerchenfeldstrasse 5, 9014 St. Gallen, Switzerland

ARTICLE INFO

Keywords:

Volatile amines
Donor-acceptor Stenhouse adducts (DASAs)
Electrospinning
Colourimetric detection
Biomedical sensors

ABSTRACT

Volatile amines are present in our daily life as a result of chemical manufacturing, agriculture and farming, release by rotten food or exhalation under certain medical conditions or diseases. An efficient, fast and low-cost method for detecting these compounds is desired due to their often-toxic nature. The development of a highly sensitive electrospun colourimetric sensor for the detection of volatile amines is reported here. Composite microfibrous meshes were obtained by incorporating activated furan adducts (FAs) into electrospun polymer meshes. Volatile amines penetrate into the amorphous polymer matrix where the ring-opening reaction with FAs yields strongly coloured donor-acceptor Stenhouse adducts (DASAs), resulting in an easily observable visible mesh colour change. Different FAs were evaluated, including a highly reactive FA yielding 3rd generation DASAs. The colourimetric responses were assessed qualitatively and quantitatively by RGB (red, green and blue) colour analysis. The sensors showed a detection range with high sensitivity down to the low-ppb range. Additionally, the covalent attachment of FAs to a polymer backbone anchored them inside the fibres and successfully prevented leaching. Thus, the cytotoxic effect of leached FAs was eliminated, as shown by indirect and direct contact tests with human fibroblasts.

1. Introduction

Chemical gas sensors that can reliably detect small quantities of volatile amines are required for a wide range of different applications [1–4]. Volatile amines are used at a large scale in the chemical industry for producing rubbers, herbicides and pharmaceuticals, and extensively in research laboratories. Their toxicity presents serious workspace safety hazards [1]. Furthermore, amines are common structural motifs in illegal drugs, such as methamphetamine [2], and several volatile amines, including di- and trimethylamine, have been identified as diagnostic disease markers in exhaled breath for diseases such as chronic kidney disease or respiratory infections [3–5]. For many of these applications in workplace exposure monitoring, drug detection and

diagnostic screening, colourimetric sensors and indicators with a strong visual response are particularly useful since they can be employed as quick point-of-care tests [6]. They provide a fast warning to users, such as exposed workers or law enforcement personnel, about the presence of the amines without the need for elaborate analytical equipment. Ideally, such sensors should combine high sensitivity, specificity, reliability and short response time with very low manufacturing costs, which enables a single-use concept.

For colourimetric amine sensors, active sensing compounds are required that drastically change their colour upon contact to the analyte, either through non-covalent interaction or chemical reactions yielding highly coloured compounds. Several examples of colourimetric amine sensors have been reported recently for monitoring food quality [7–11]

Abbreviations: DASA, donor-acceptor Stenhouse adduct; DEA, diethylamine; DMA, dimethylamine; FA, furan adduct; hDF, human dermal fibroblasts; PCL, polycaprolactone; PLLA, Polylactic acid

* Corresponding author.

E-mail address: luciano.boesel@empa.ch (L.F. Boesel).

¹ These authors contributed equally.

<https://doi.org/10.1016/j.snb.2020.128570>

Received 9 March 2020; Received in revised form 5 June 2020; Accepted 7 July 2020

Available online 09 July 2020

0925-4005/ © 2020 The Author(s). Published by Elsevier B.V. This is an open access article under the CC BY license (<http://creativecommons.org/licenses/by/4.0/>).

or biomedical relevant volatile amines [12,13]. Yet, few colourimetric indicators exist that are highly specific for amines, with many responding non-specifically to changes in pH or providing a colour response which cannot be easily discriminated by the human eye. Some of the reported indicators or sensors also require complicated synthesis steps or are not sensitive enough for sub-ppm detection of amines. A specific and strong colour reaction with much promise to overcome these limitations is the ring-opening reaction of amines with activated furan adducts (FAs), which yields donor-acceptor Stenhouse adducts (DASAs), a new class of organic photo-switches with extremely strong purple-blue colouration (extinction coefficient $\sim 100,000 \text{ M}^{-1}\text{cm}^{-1}$) [14–17]. Importantly, this colour reaction is highly specific to amines, occurring most strongly with secondary alkyl amines [17]. Recently, Read de Alaniz et al. demonstrated the high potential of the DASA reaction for sensor applications with the detection of a range of different amines in solution and, after simple impregnation of nylon filters with the FAs, even in the gas phase [18,19].

The development of DASA-based volatile amine sensors requires facile, stable and scalable incorporation of FAs into a sensor matrix that meets the requirements of the DASA reaction while providing quick access for the volatile amines through high porosity and surface-to-volume ratio and short diffusion lengths through a polymer matrix. Electrospun meshes represent especially promising candidate substrates for high-sensitivity sensor applications due to their high porosity and surface-to-volume ratio, their facile fabrication, the wide range of processable polymers and the ease of doping them with active compounds [20–22]. Electrospun meshes have found use in different chemical sensor applications, such as for gaseous ammonia [23], aliphatic amines [24,25], solvents [26], and nerve gas agents [27], among others, and their use in colourimetric sensors has recently been reviewed [28].

Another important aspect of DASA-based sensors is the choice of FAs that meet the required colour and reactivity profiles. Recently, Read de Alaniz et al. developed new and highly reactive FAs for the 3rd generation of DASA, which may have strong implications for high-performance sensors [29]. However, to be used for diagnostics applications in contact with human skin, the so far unknown toxicity of the FA's and their tendency for leaching from the sensor matrix must be assessed.

In this paper, we report the development of highly sensitive volatile amine sensors based on porous electrospun fibrous meshes with FAs incorporated inside the polymeric fibre matrix. The ability of the sensors containing different FAs to detect a range of relevant aliphatic amines and ammonia was investigated and sensitivity down to the ppb range via 3rd generation FAs was demonstrated. Furthermore, it was demonstrated that the covalent fixation of FAs by co-electrospinning polymer-conjugated FAs can effectively solve their leaching from the fibres and avoid the risk of cytotoxicity.

2. Experimental

2.1. Materials

Polycaprolactone (PCL) ($M_n = 80\,000 \text{ g/mol}$), Tetrahydrofuran (THF, inhibitor-free), Chloroform (CHCl_3), Diethylamine (DEA), Dimethylamine (DMA, 40 wt% in H_2O), Diethanolamine, Dicyclohexylamine, Diisopropylamine and N-methyl-phenethylamine were obtained from Sigma-Aldrich, Fischer Scientific or Merck; Methanol from Fischer Scientific; *N,N*-Dimethylformamide (DMF) from VWR Chemicals; and Dichloromethane (DCM) from Macron fine chemicals. Polylactic acid (PLLA) (Ingeo™ Biopolymer 2500HP) and Polylactide acid (PLLA) (Ingeo™ Biopolymer 3100HP) were obtained from Natureworks (Switzerland).

2.2. Fabrication

2.2.1. FA synthesis

The activated furan adducts 5-(furan-2-ylmethylene)-2,2-dimethyl-1,3-dioxane-4,6-dione (Meld), 5-(furan-2-ylmethylene)-1,3-dibutylpyrimidine-2,4,6-(1H,3H,5H)-trione (Barb), and 4-(furan-2-ylmethylene)-2-phenyl-5-(trifluoromethyl)-2,4-dihydro-3H-pyrazol-3-one (PyraF) were prepared according to procedures described in the literature [14,29]. All spectroscopic data matched reported values. ^1H NMR spectra of the three compounds are shown in Fig. S1.

The synthesis and the properties of the Meld-functional copolymer (PMeld) polymer have been reported before [19]. The polymer was obtained with the following specifications: $M_n = 27 \text{ kDa}$, $\text{PDI} = 1.4$ (GPC); the Meld-functional monomer to co(monomer) ratio was 4:1. The ^1H NMR data matched the specified copolymer ratio (Fig. S2).

2.2.2. Electrospinning solutions

Clear PCL solutions were prepared by dissolving the polymer in $\text{CHCl}_3\text{:MeOH}$ (9:1 by volume for 12 or 20 w/v% PCL solutions and 4:1 for 10 w/v%) using a shaker at room temperature for 2 days.

For adding the FAs, 0.36 mol L^{-1} stock solutions in DCM were prepared for Meld (80 g L^{-1}), Barb (114 g L^{-1}), and PyraF (110 g L^{-1}). The Meld stock solution was added to the PCL solution for a PCL/Meld weight ratio of 100:1. Using equal molar amounts for Barb and PyraF resulted in a slightly higher PCL/FA weight ratios (both 100:1.4). PCL meshes with higher PCL/Meld ratios (100:3 for PCL-M3 and 100:5 for PCL-M5) were prepared analogously. Solution preparation and electrospinning of PLLA fibres are described in the supporting information.

For electrospinning solutions of PMeld and PCL blends, both polymers were dissolved in $\text{CHCl}_3\text{:MeOH}$ (9:1 by volume). The addition of PMeld was calculated to provide an amount of Meld functionality equivalent to a 100:1 or 100:5 Meld/PCL ratio. For example, 600 mg of PCL was mixed with 55 mg of PMeld ($\sim 117 \text{ mmol}$ Meld functional groups) and dissolved in 5 mL of $\text{CHCl}_3\text{:MeOH}$ 9:1 for a $\sim 100:1$ PCL/Meld ratio.

2.2.3. Electrospinning

A custom-made electrospinning set-up was used. Briefly, an infusion pump (AL1000-220, WPI, USA) provided a constant flow through a plastic syringe equipped with a stainless steel blunt needle (inner diameter of 0.8 mm). Positive and negative voltage supply sources (AIP Wild AG, Switzerland) were connected to the needle and the collector, respectively. The electrical field strength was controlled using LabView software (National Instruments, USA). The whole apparatus was placed in a grounded Faraday cage inside a fume hood with the whole setup located in a climatic chamber, which provided controlled environmental conditions (maximum tolerated deviations of $\pm 0.5^\circ\text{C}$, $\pm 5\%$ RH).

The meshes were electrospun for 15 min under ambient conditions (flow rate: $30 \mu\text{L min}^{-1}$; voltage: $+12.5/-5 \text{ kV}$ at the needle tip and collector; needle tip-collector distance: 18 cm; relative humidity $\sim 40 \pm 5\%$). For obtaining thicker meshes, the electrospinning time was increased to 30 min, 60 min or 150 min, with the last ones used for cytotoxicity evaluations. Table 1 summarizes the designations of the samples used in this work.

2.3. Colourimetric detection by electrospun sensors

For amine sensing, DEA solutions were prepared in DCM in concentrations ranging from ~ 0.001 to $5 \mu\text{mol mL}^{-1}$. For a testing volume of 120 mL, $10 \mu\text{L}$ of the stock solutions were added for amine concentrations in the gas phase ranging from 2 ppb to 10 ppm. Higher concentrations (20 and 40 ppm) were tested by adding neat DEA ($10 \mu\text{L}$ and $20 \mu\text{L}$, respectively). Stock solutions of other amines were prepared at $5 \mu\text{mol mL}^{-1}$. For amines provided in aqueous solution, DCM was replaced by acetone or THF.

Table 1

List of samples used in this study.

Sample's name	Polymer and concentration (w/v)	FA type	Polymer/FA weight ratio
PCL	PCL 12 %	–	–
PCL-M1	PCL 12 %	Meld	100:1
PCL-M3	PCL 12 %	Meld	100:3
PCL-M5	PCL 12 %	Meld	100:5
PCL-B	PCL 12 %	Barb	100:1.4
PCL-P	PCL 12 %	PyraF	100:1.4
sPCL-M1*	PCL 10 %	Meld	100:1
bPCL-M1*	PCL 20 %	Meld	100:1
PLLA-M1	PLLA 14 %	Meld	100:1
PCL-PM1	PCL/PMeld 12 % / 1.1 %	–	100:1
PCL-PM5	PCL/PMeld 12 % / 5.5 %	–	100:5

* "s" and "b" mean small and big fibre, respectively (see Fig. S13c).

Circular specimens (\varnothing 6 mm) were cut from the electrospun meshes. One specimen per measurement was attached with adhesive tape near the top of a glass Erlenmeyer flask equipped with a glass stopper (120 mL total volume). The stock solution of the volatile amines was added to the bottom of the flask and the flask was immediately closed. The specimens were exposed to the amine vapour for 30 min under ambient conditions and normal daylight conditions, unless otherwise specified.

2.4. Colour quantification and analysis

The coloured meshes were removed from the flasks and placed on a white paper for analysis. The specimens were left in a fume hood for 20 min under aluminium foil to allow possible residual volatile compounds to evaporate. Subsequently, the specimens were photoscanned (Epson Perfection V550 Photo, Seiko Epson Corporation, Germany). The RGB values of the photoscans were analysed using MATLAB (Version 3.10.12). The colour intensities, with their standard deviations, in RGB colour coordinates were obtained over all pixels of a line drawn over the length of the whole specimen. The magnitude of colour change relative to an unused reference specimen of the same type was calculated as the Euclidian distance in the 3-dimensional RGB colour space (ARGB):

$$\Delta RGB = \sqrt{(R_s - R_{ref})^2 + (G_s - G_{ref})^2 + (B_s - B_{ref})^2} \quad (1)$$

with R, G and B being the obtained red, green and blue values, respectively, and the subscripts *s* and *ref* indicating sample and reference, respectively. The RGB values of pristine Meld- and Barb-based meshes were 255/255/255, i.e. white, and for pristine PyraF the RGB values were 212/197/13, i.e. mustard yellow (for the MATLAB code, see SI "MATLAB code for RGB measurements").

2.5. Characterization

The fibre morphology was characterized by scanning electron microscopy (SEM) (Hitachi S-4800, Hitachi High-Technologies, USA & Canada) using a 2 kV accelerating voltage and a 10 μ A current flow. Electrospun meshes were sputter-coated with gold (5 nm thickness, EM ACE 600, Leica Microsystems, Switzerland) prior to imaging. For cross-section images, the specimens were cut with a surgical blade. Mean fibre diameters and thicknesses were calculated based on 100 fibres and 40 cross-section measurements from the SEM micrographs using Image J software (version 2.35).

The reflectance response of the colourimetric meshes was measured using an Olympus IX-81 inverted microscope with one of its outputs coupled to an Andor Shamrock 303i equipped with an iDUS CCD DV420A-OE camera. No filter was applied. Full Vertical Binning (FVB) was the read mode used. A sample of TiO₂ was used as a white reference.

Differential scanning calorimetry (DSC) curves were recorded on a NETZSCH DSC 214 Polyma (NETZSCH, Germany) under a nitrogen atmosphere at a heating rate of 10 K min⁻¹ and analysed using the associated software (NETZSCH Proteus Thermal Analysis, Version 7.1.0). The temperature ranges were -65 to 100 °C for PCL meshes and pellets, -2 to 140 °C for a PLLA mesh, and -65 to 140 °C for PMeld. For all but PMeld, the first heating cycle was analysed. For PMeld, a second heating cycle was analysed. The T_g was determined as the middle point of the observed transitions.

Attenuated total reflection Fourier-transform infrared (ATR-FTIR) spectra were recorded on a Varian 640-IR FTIR spectrometer equipped with a diamond crystal insert between 4000 and 650 cm⁻¹ with a resolution of 2 cm⁻¹. ¹H NMR spectra were recorded at 400.2 on a Bruker Avance III 400 NMR spectrometer at 298.2 K. The ¹H NMR spectra were referenced internally with residual resonances of the solvent CDCl₃.

2.6. Cytotoxicity assay

The cytotoxicity of electrospun meshes was assessed by indirect and direct contact tests with human dermal fibroblasts (hDF, cat. HDFp, Lot. EB1104281, juvenile donor, CELLnTEC). For the indirect test, extracts of washed and unwashed PCL-M1/M5 and PCL-PM1/M5 were evaluated. To prepare the extracts, ~10 mg pieces were placed in Eppendorf tubes and incubated in 1 mL of culture medium (Dulbecco's Modified Eagle's Medium, high glucose (DMEM) supplemented with 10 v/v% foetal calf serum (FBS), 1 % Penicillin-Streptomycin-Neomycin (PSN) and 2 % L-Glutamine) for 24 h at 700 rpm and 37 °C. Culture medium incubated for 24 h without mesh pieces was used as a control. In case of washed meshes, specimens were pre-incubated in 1 mL of 100 % ethanol on a shaker overnight at 700 rpm and 37 °C prior to the extraction in a culture medium.

hDF cells were seeded in 96-well plates at a density of 5 × 10³ cells/well in culture medium and incubated at 37 °C in standard cell culture conditions (95 % air/5 % CO₂) for 24 h. Thereafter, the medium with material extracts was replaced with material extracts for 24 h in standard culture conditions before assessing cell metabolic activity using the alamarBlue® assay (LifeTechnologies, Thermo Fisher Scientific, Switzerland). In brief, cells were incubated for 4 h at 37 °C in 10 v/v% Alamar Blue in a fresh culture medium. Fluorescent excitation and emission were measured at λ_{ex} = 540 nm and λ_{em} = 580 nm (Mithras2 Plate reader, Berthold Technologies, Germany) and the obtained values were normalized to those of hDF cultured in a fresh culture medium. The total cell number was evaluated with a DNA binding fluorescent dye (Bisbenzimidazole, Hoechst 33258, Sigma-Aldrich, Switzerland). For this, well-plates were washed 3 times with pre-warmed PBS before adding 100 μ L of double-distilled H₂O. After 2 freeze-thaw cycles (-20 °C), 100 μ L of Hoechst (1:50 dilution in TNE buffer) were added and the fluorescence intensity was quantified at λ_{ex} = 485 nm and λ_{em} = 528 nm on a multiwell microplate reader (Mithras 2, Berthold Technologies, Germany). The DNA concentration for each sample was calculated using a standard calibration curve made with calf thymus DNA. Three independent experiments with three replicates per group were performed. All values are expressed as mean \pm sd. Data from both tests were analysed with GraphPad PRISM (version 8.0). The statistical analysis was performed using ANOVA with Tukey's post-hoc test and statistical significance was set at * p < 0.05, ** p < 0.01, *** p < 0.001 and **** p < 0.0001.

For direct contact tests, hDF was cultured directly on PCL-PM1 and PCL-PM5 meshes (previously washed with 100 % ethanol). For this, 8 mm diameter specimens were sterilized with UV irradiation and fixed with a silicon ring and glass tube in 48-well cell culture plates. hDF was seeded at a density of 2.038 × 10⁵ cells/well in 30 μ L of culture medium and allowed to adhere for 2 h prior to the addition of 270 μ L culture medium. After incubation for 24 h at standard culture conditions, cell morphology was assessed by fluorescence microscopy. For this, samples were washed 2 times with PBS, fixed with 4 v/v%

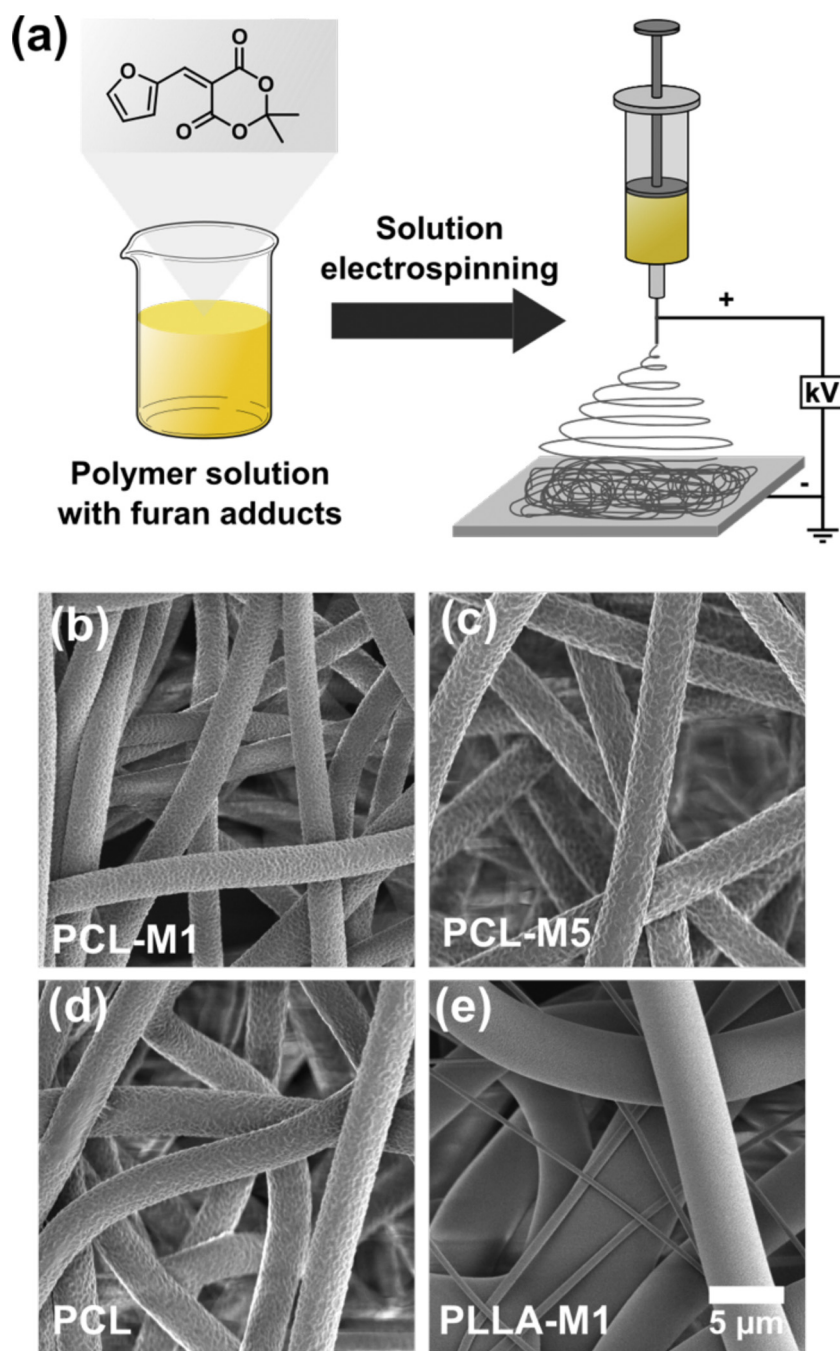


Fig. 1. (a) Schematic depiction of the fabrication process of electrospun meshes doped with activated FA Meld. (b–c) SEM images of electrospun meshes with PCL/Meld ratios of 100:1 (PCL-M1) and 100:5 (PCL-M5), respectively. (d) SEM image of PCL fibre mesh without Meld; and (e) SEM image of a PLLA-M1 (PLLA/Meld ratio 100:1) mesh.

paraformaldehyde (PFA, Sigma-Aldrich, USA) for 10 min at room temperature and incubated in 5 % Goat/1 % BSA v/v in PBS for 30 min at room temperature. After 3 washing steps with PBS, the samples were incubated in 200 µl of 1 % BSA in PBS supplemented with 4',6-diamidino-2-phenylindole (DAPI, 1:4000 v/v, Biotium, USA), and Alexa546-labelled Phalloidin (1:150 v/v, Thermofischer, USA) for 1 h at room temperature, under agitation ($150 \text{ U} \cdot \text{min}^{-1}$) and protected from light. Samples were rinsed 3 times with PBS, mounted on microscopic slides and imaged using a confocal microscope (LSM 780, Carl Zeiss, Germany). Three independent experiments with duplicates per group were performed.

3. Results and discussion

3.1. Design and fabrication of electrospun sensor

For a homogeneous colour response from an electrospun sensor, the active compounds have to be homogeneously distributed throughout the polymer fibres and the mesh. To this end, FAs were dissolved in the PCL or PLLA polymer solutions at defined polymer/FA ratios and the solutions were electrospun to yield FA-doped fibrous meshes (Fig. 1a). With the good solubility of all components in the solvents used, electrospinning was expected to result in the homogeneous dispersion of the FAs inside the fibres. The convenience of this process combined with the ease of varying the polymer/FA ratio and the FA and polymer

type made it ideal for developing and assessing this new sensor system, though the lack of covalent FA attachment may present drawbacks in terms of leaching [28]. First, we focused on the Meldrum's acid-based FA Meld, which has been more extensively used for synthesising DASAs and for a first amine sensing study [18]. It combines a facile one-step synthesis from cheap starting materials with a high reactivity and the bright pink colour of its alkyl amine-based DASAs [17].

While electrospun meshes provide a high surface-to-volume ratio and respective high porosity into which volatile compounds or cations in an aqueous environment can easily penetrate [16,30,31], diffusion of the amines into the fibres is required for a colour reaction and, therefore, the polymer properties must facilitate this permeation. The hydrophobic semi-crystalline polyester poly(ϵ -caprolactone) (PCL) was selected for its properties. It combines a crystalline phase ($T_m \sim 60^\circ\text{C}$) that provides mechanical stability and fibre integrity at room temperature and an amorphous phase with a glass transition temperature (T_g) of only about -60°C , allowing dynamic mobility on the molecular level [32]. A further benefit is the excellent electrospinnability of PCL, which enables obtaining different morphologies, and its miscibility with small molecular compounds as well as various other polymers [30,33]. The aprotic nature of PCL can provide a benign environment for the DASAs, which have been reported to be compromised in protic environments [34]. Finally, PCL is a widely used polymer in electrospinning meshes for biomedical applications [35,36]. For a comparison with a structurally closely related but high- T_g polymer, we also used poly(L-lactic acid) (PLLA, $T_g \sim 60^\circ\text{C}$, $T_m \sim 175^\circ\text{C}$) [37,38].

Electrospinning PCL or PLLA with Meld in a 100:1 wt ratio resulted in white meshes with macroscopically flat and homogeneous surfaces. The fibre morphology was investigated by SEM, revealing uniform fibres with $2.7 \pm 0.5\ \mu\text{m}$ diameters for PCL-M1 (Fig. 1b). Fibres with smaller and larger diameters were obtained by controlling the solution concentration (Table 1 and Fig. S13c). The incorporation of Meld had no observable influence on the fibre morphology or diameter, as evidenced by comparison with fibres from neat PCL and fibres with a 5 times higher Meld incorporation (100:5) (Fig. 1c/d). PLLA meshes were found to be composed of a mixture of thinner and thicker fibres, which might derive from the formation of a secondary jet at the needle tip (Fig. 1e). To confirm the Meld incorporation, the meshes were characterized by FTIR spectroscopy. Meld on its own has a distinct peak at $1580\ \text{cm}^{-1}$ that appeared in the electrospun meshes, at $1591\ \text{cm}^{-1}$ for the PCL-M1 and more prominently for PCL-M5 (Fig. S3), indicating effective incorporation. We employed DSC to assess the thermal properties of the PCL and PLLA meshes (Figs. S7 and S8) and found no distinct differences in melting behaviour between PCL meshes with or without Meld incorporation. The DSC results for PLLA fibres showed the typical phase transitions with a glass transition and an endothermic peak from the enthalpic relaxation of the PLLA mesophase ($\sim 67^\circ\text{C}$), a distinct cold crystallization peak at 92°C , and the melting transition ($T_m = 176^\circ\text{C}$, Fig. S8).

3.2. Volatile amine sensing

To test the ability of Meld-doped PCL meshes to detect volatile amines, we used a closed setup containing a defined amount of DEA vapour specimen. DEA is an excellent model amine due to its high vapour pressure ($\text{bp} = \sim 55^\circ\text{C}$) and alkyl amine structure [18]. Within 10 s of exposure, the initially white specimen started to acquire a homogeneous, pink colour that increased quickly in intensity and was easily observable by the naked eye (Fig. 2a). The colored DASA is formed due to the ring-opening of Meld upon reaction with DEA at room temperature in the absence of catalysts or other reagents (see Fig. S12a for the reaction scheme). It should be highlighted that such a DASA sensor is not based on an equilibrium reaction but reacts as long as amines and unreacted FAs are present, continuously increasing the colour intensity. Importantly, the sensing did not result in any observable morphological differences in the fibre (Fig. S10). The sensing

experiments were conducted under ambient light conditions and the colour intensity of the specimen did not increase when left in the dark (Fig. S11b). Generally, DASAs from alkyl amines possess very little photo-switching ability in anything but aromatic solvents [14,16]. However when directly illuminated by a stronger light source (desk lamp) for a longer time period, a slight colour reduction was observed, showing that light may influence the colour through DASA photo-switching and should be minimized (Fig. S11a). The PLLA mesh was tested under the same conditions but did not show any colour development, even at a higher DEA concentration. This indicates that a glassy amorphous phase effectively hinders the penetration of volatile compounds into the fibres, underlining the importance of a low- T_g amorphous phase, such as in PCL, for the polymer matrix.

A strong colour response that is easily detectable by the naked eye is essential for potential sensor applications in workplace safety, drug detection and point-of-care diagnostic screening, where a clear on/off difference must be detected. However, quantification of the colour response provides more in-depth information to the user and allows assessing the sensor accuracy, detection range and performance. Ideally, quantification of the colour response should be easy to interpret (i.e. the colour response must be directly correlated to the amine concentration) and non-demanding regarding the required instrumentation. To this end, we photoscanned the specimens on a commercial photoscanner 20 min after the end of each experiment to obtain digital colour images under highly repeatable lightning conditions and performed a quantitative red-green-blue (RGB) analysis. The RGB system was used since the colour space commonly used to display colours on digital devices is ideal for such an analysis. This methodology is the standard method used in radiation therapy dosimetry to determine the absorbed dose and dose distribution of ionizing radiation [39], making it a suitable method for biomedical evaluation. Average RGB values (0–255) were obtained over pixels for a line across the whole sensor area. To convert the obtained three RGB values into a single representative value, the distance ΔRGB for a mesh before and after sensing in the RGB vector space was calculated, as shown in Eq. (1). The ΔRGB can range from 0 to 442, with the highest value corresponding to a white-black transition. For the completely white PCL/Meld-based meshes (measured RGB 255/255/255) the analysis was simple. However, the ΔRGB analysis can also be used for meshes that already possess an intrinsic colour since it represents colour differences. We combined the RGB analysis with surface reflectance spectroscopy to investigate the spectral properties behind the colour response of the sensors. First, we investigated the sensor response for two DEA concentrations over time. The colour response of the mesh increased steadily over time, corresponding to a single DASA peak that was centred at 537 nm in the reflectance spectrum (Fig. 2b), close to the 545 nm reported for this DASA type in toluene solution [17]. Notably, the peak height increased over time, yet the peak position was not shifted. The appearance of the DASA absorption correlated to a steady increase in ΔRGB over time, with the rate of colour formation depending on the amine concentration (Fig. 2c).

The performance of sensors with a continuous sensing reaction differs distinctly from equilibrium-based sensors. For the latter, constant colour results after a certain equilibration time and can be correlated to the analyte concentration. The strength of a continuous sensing reaction, on the other hand, lies in the accumulative nature of the sensor response. Thus, the weak signal of a very low analyte concentration can be intensified by increasing the exposure time or repeatedly exposing the mesh to the same conditions, whereas shorter exposure times can be selected for higher concentrations. This sensor type has the benefit of providing information to the user about the total exposure, comparable to a dosimeter, especially in applications such as workplace chemical exposure monitoring. However, for a quantitative concentration measurement, the exposure time must be strictly controlled to achieve comparable results; we, therefore, selected an equilibrium exposure time of 30 min.

The results for two DEA concentrations in a surface reflectance

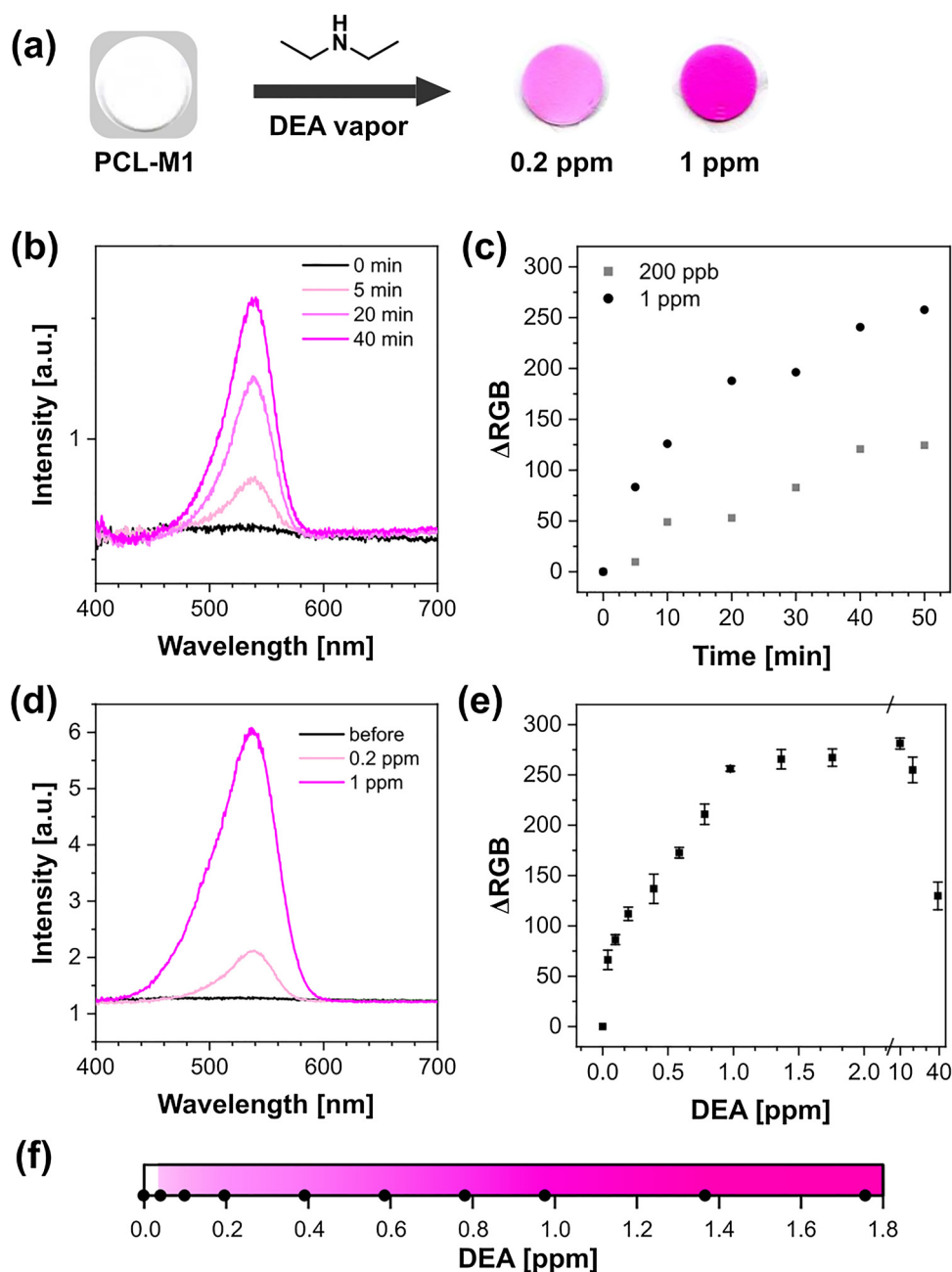


Fig. 2. (a) Photoscanned images of PCL-M1 pieces (Ø 6 mm) before and after exposure to DEA vapor for 30 min. Reflectance spectra (b) and ΔRGB colour response (c) of PCL-M1 specimens exposed to 1 ppm DEA for different time periods. (d) Reflectance spectra for PCL-M1 specimens before and after exposure to two DEA concentrations for 30 min. (e) ΔRGB colour response of PCL-M1 specimens exposed to a range of DEA concentrations for 30 min. Linear regression for DEA concentration 0–1 ppm: $\Delta RGB = 218[\text{DEA}] + 47$ ($S = 23$, $r^2 = 0.932$) (f) Visual response of PCL-M1 sensor to varying DEA concentrations.

spectrum and for a series of ΔRGB colour response measurements at DEA concentrations ranging from 0.04 ppm to 40 ppm are presented in Fig. S12b. The corresponding RGB values are shown in Fig. S12b. For visualization, a colour bar shows the measured colours corresponding to the different values (Fig. 2f). Strikingly, a distinct pink colour is already clearly observable by the naked eye at a concentration of 0.04 ppm. It is important to mention that the color evolution is a result only of the reaction between Meld and DEA, as Meld is stable in the presence of non-nucleophilic solvents such as DCM (Fig. S12c). The corresponding ΔRGB values increase up to a concentration of about 1 ppm, after which only a slight increase was found until 10 ppm. Accordingly, the colour can be linearly correlated to the amine concentration up until the plateau is reached in the range of 0–1 ppm (see the caption to Fig. 2e). At very high concentrations above 20 ppm, the

response is declining due to the nucleophilic degradation of the DASAs by the excess of amine, defining the upper limit of the sensor (Fig. S12d-g). However, it should be noted that when monitoring high concentrations, the sensor response could hardly be confused with that of a lower concentration since the sensor would reach a maximum before the subsequent drop-off in colour.

After assessing the performance of PCL-M1, we investigated the influence of different parameters on the sensing process. Sensor performances are usually affected both by physical and chemical factors, such as the density of reactive sites, surface-to-volume ratio, sensor geometry, transducer reactivity and analyte properties.

The first parameter assessed was the Meld concentration inside the fibres, which can result in a higher DASA concentration and, thus, influence the sensor response. We tested specimens with PCL/ Meld ratios

of 100:1/3/5 (Fig. S13a) and found an increase in the ΔRGB value by ~ 110 units (+44 %). Higher Meld concentration resulted in the increasingly red colour of the meshes, corresponding to a lower blue value (Fig. S13b). This result confirms that the concentration of reactive units (Meld molecules) correlates with the colour change and could, therefore, be used to tune the sensitivity and colour response of the electrospun sensor.

Another parameter of importance is the diameter distribution of the fibres within the electrospun meshes (Fig. S13c), which influences the surface-to-volume ratio. Surprisingly, we found a 36 % reduced colour response for the thinnest fibres ($1.1 \pm 0.6 \mu\text{m}$, sPCL-M1), possibly due to larger amounts of crystalline oriented phases within the polymeric fibres, caused by higher drawing ratios during the fibre formation process leading to fibre diameter reduction [40,41]. Wong et al. found a decrease of PCL fibre crystallinity from 50 to 42 % when the diameter was increased from 200 nm to 900 nm [40]. This is in contrast to the expected increase in surface area and reduction in diffusion length of the amine inside the fibres, which would lead to higher sensor sensitivity. Larger diameters ($4.0 \pm 0.3 \mu\text{m}$, bPCL-M1) resulted in little change in the sensor response.

We also tested the influence of the thickness and the applied area of the electrospun mesh but found no or little influence (Fig. S14). This is clearly advantageous, demonstrating that the high porosity of the meshes allows diffusion of the analyte even in thicker constructs. Changes in the relative environmental humidity between 20–85% also resulted in no distinguishable differences in the sensor response (Fig. S13d), which is in line with previous reports that showed a limited influence of water on the DASA reaction with only a slight increase in reactivity [18].

The effects of analyte properties, such as nucleophilicity, steric hindrance, volatility, size, and hydrophobicity of the amines, on sensing were also investigated. Fig. S15 shows the investigated amines and the response of fibre meshes to 1 ppm of each of them when compared to DEA. Although this data only gives qualitative information on the effect of analyte type, it is clear that secondary alkylamines (DMA, DEA, etc.) possess the highest reactivity and, therefore, induce the strongest signal, whereas less nucleophilic secondary amines, such as N-alkylanilines, were less reactive. Ammonia and primary amines (e.g., n-butylamine) were also considerably less reactive or not at all. The response of secondary amines depended on the structure, with an increase in amine size leading to a weaker response. Cyclic secondary amines, such as morpholine and pyrrolidine (data not shown), reacted strongly but resulted in a more orange colour after starting with the usual pink, possibly due to DASA degradation by these extremely nucleophilic amines, what has been reported before [17].

3.3. Effect of FA type on sensor performance

The properties of DASAs, such as their colour and the rate of the DASA reaction, strongly depends on the FA structure. Recently, the Read de Alaniz group reported a series of highly reactive FAs for synthesising 3rd generation DASA that, in addition to their spectral properties with strong bathochromic shifts, were reported to provide a much increased reactivity towards amines [29]. For a comparison of FA sensing performance, we selected the pyrazolone-based 3rd generation FA, PyraF (Fig. 3a), and the 1st generation N-substituted barbituric acid FA, Barb. Incorporation of Barb and PyraF into PCL meshes at the same molar concentration as in PCL-M1 yielded meshes PCL-B and PCL-P with homogeneous fibres and comparable fibre morphologies to PCL-M1 (Fig. 3a, FTIR spectra of FAs and meshes in Fig. S4/5). The only notable difference was the distinct yellow colour of the PCL-P mesh due to the strong colour of PyraF (Fig. 3b). Exposure to DEA vapour resulted in a pinkish colour for PCL-B, with a colour intensity notably below that of PCL-M1. For PCL-P, we found a strong change from the initial yellow to a very strong blue-purple, translating in a large change in ΔRGB at 0.2 ppm DEA concentration. This change only marginally increased at

1 ppm, indicating a very high sensitivity due to the high PyraF reactivity (Fig. 3b). The reflectance spectra of PCL-B revealed the expected low peak intensity of DASA absorption (Fig. 3c). For PCL-P, it revealed a distinct peak of the unreacted PCL-P around 460 nm, corresponding to the initial yellow colour of the mesh. The DASA reaction resulted in the reduction and, finally, the disappearance of this peak and the appearance of a corresponding DASA peak around 560 nm. The disappearance of the 460 nm PyraF reflectance peak indicates complete consumption during the sensing reaction. Due to the high sensitivity of PyraF, we tested the mesh in a lower concentration range between 2 ppb and 1 ppm. The results for PCL-P together with the results for PCL-M1 (for comparison) are presented in Fig. 3d. The difference between the meshes is striking, with PCL-P resulting in a ΔRGB of 74 at a DEA concentration of 10 ppb and reaching a plateau at 100 ppb. Accordingly, the sensitivity of electrospun sensors can be much improved with the use of highly reactive 3rd generation FAs. Due to the early ΔRGB plateau at very low amine concentrations, the PyraF-based mesh essentially gives a highly sensitive off-on response to the presence of volatile amine, whereas the colour response of Meld provides more differentiated information about the amine concentration over a much larger concentration range. The combination of two or three FAs in a sensor would, therefore, provide both highly sensitive early detection of volatile amines and additional insight into their concentration. This combination could also extend the detection limit of the sensor by taking advantage of the reactivity of the different FAs. E.g., for DEA, a single sensor could be used with PyraF to detect concentrations lower than 0.1 ppm, Meld for lower than 1 ppm, and Barb for 1–10 ppm.

3.4. Use of covalently-bound FA to avoid leaching

The potential use of an electrospun amine sensor as a quick test in different applications for workspace safety, medical screening or drug testing brings strong demands regarding leaching FAs from the fibrous meshes in contact with sweat on the skin and the potential toxicity of the FAs. We tested leaching from the specimens by washing PCL-M1 in water or ethanol followed by drying and subsequent exposure to DEA vapour. After washing in either solvent, PCL-M1 lost its ability to generate a colour response, indicating complete removal of Meld from the fibres during washing (Fig. 4a). We hypothesized that covalently attaching the FA to the polymer inside the fibre could overcome this leaching challenge. Recently, we developed a new Meld-functional copolymer via ring-opening metathesis polymerization (ROMP) [19]. We blended such a ROMP copolymer PMeld (Fig. 4b), with ~ 20 % Meld-functional monomer units, with PCL in a ratio that provided approximately the same amounts of Meld functional group in the fibres as in PCL-PM1 and PCL-PM5. The resulting white meshes possessed homogeneous fibre morphologies (Fig. 4c) close to the pure PCL/Meld fibres. The characteristic FTIR peak of Meld was present both in the spectrum of the PMeld copolymer as well as on those of the meshes containing it (Fig. S6). DSC analysis did not show an independent glass transition for the PMeld polymer ($\sim 71^\circ\text{C}$) inside the fibres, indicating good blending with the PCL (Fig. S9). The sensor performance of the meshes was tested against DEA vapour, resulting in a clear colouration, though the colour response was lower, with only PCL-PM5 resulting in a colour intensity comparable to PCL-M1, possibly due to reduced accessibility of the Meld groups in the blend fibres (Fig. 4a). However, most importantly, the meshes were able to sense DEA vapour even after washing in ethanol with essentially no reduction in colouration (Fig. 4a). Accordingly, while the sensing capability of the blend fibres needs to be optimized, possibly via the structure of the ROMP polymer, these results present a clear path towards the development of highly sensitive colourimetric electrospun sensors without the danger of leachables. Given the reactivity of Meld towards amines dissolved in water [19], our results indicate that such a highly sensitive mesh could be also used to detect biomarkers in aqueous media, e.g., for bacterial vaginosis [42].

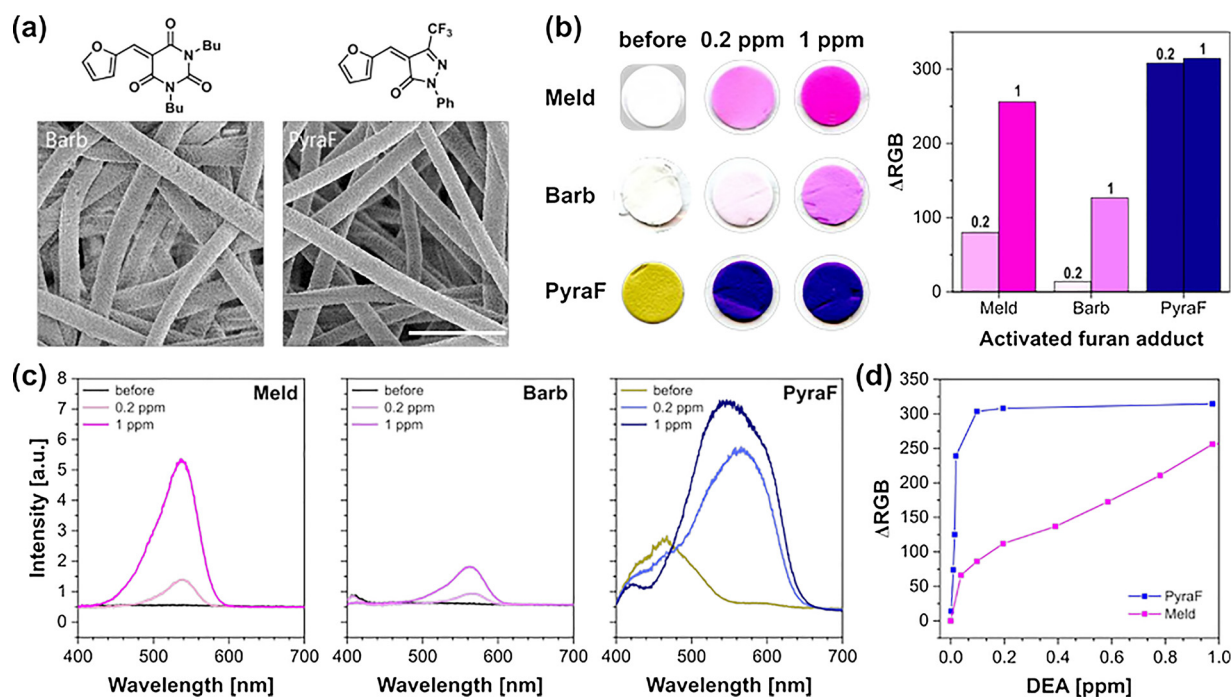


Fig. 3. (a) Chemical structures of the Barb and PyraF FAs and SEM images of PCL meshes containing them (scale bar = 10 μm). (b) Photoscans of PCL meshes containing the three different FAs exposed to two DEA concentrations (left) and the corresponding ΔRGB values (right). (c) Reflectance spectra for the three different FA meshes before and after exposure to two DEA concentrations. (d) Response of the meshes containing PyraF to different DEA concentrations. The values for PCL-M1 (containing Meld) are shown for comparison.

3.5. In vitro cytotoxicity of electrospun meshes containing FAs

Very little is known, so far, about FAs toxicity. However, applications that involve using electrospun sensors without protective gear require knowledge of any potential toxicity. We evaluated the cytotoxicity of extracts from washed and unwashed PCL-M1/M5 and PCL-PM1/PM5 meshes *in vitro* (Figs. 5a, and S16). When assessing the metabolic activity of hDF cultured with extracts of electrospun PCL-M1/

M5 and PCL-PM1/PM5 meshes, significantly lower values were observed for unwashed PCL-M5 compared to washed PCL-M5, washed/unwashed PCL-PM5 and DMEM control (Fig. 5a). While this strongly indicates that Meld FA is cytotoxic for the cells, the non-cytotoxic extracts of washed PCL-M5, in accordance with the previous section, indicates leaching Meld FA from the fibres when washed in ethanol. No significant differences were observed, regardless of washing with ethanol, between extracts of PCL-M1 and PCL-PM1 (Fig. S16), which is

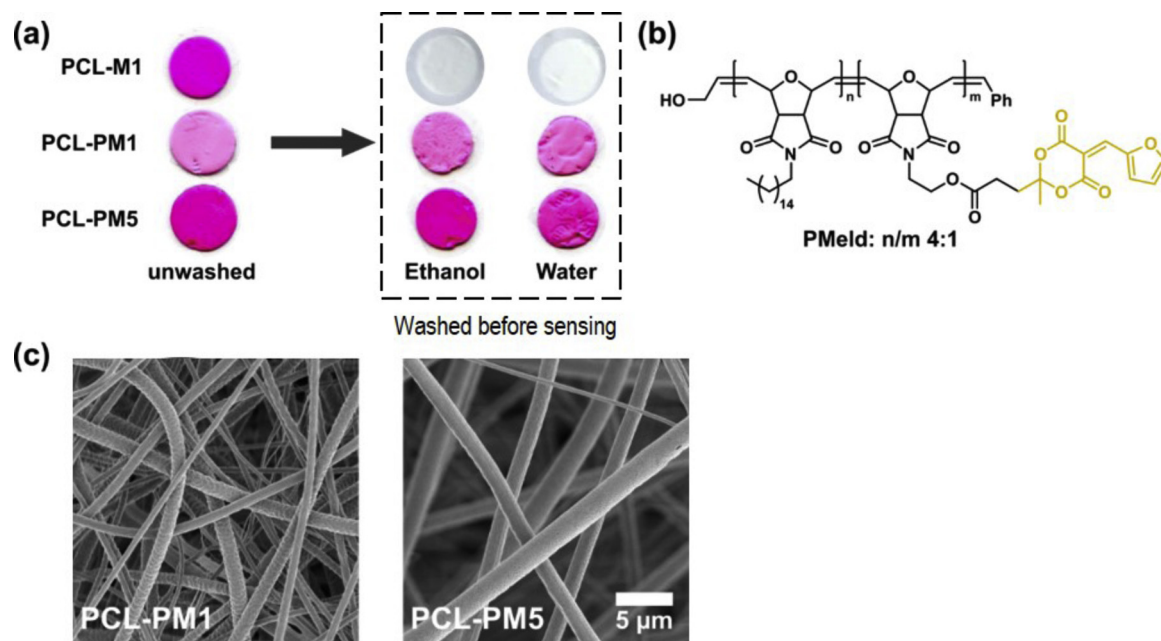


Fig. 4. (a) Photoscan of meshes with dissolved (PCL-M1) or covalently bound Meld (PCL-PM1 and PCL-PM5) after exposure to 1 ppm DEA. The meshes on the left panel were used without washing; the meshes on the right were washed in either ethanol or water and dried before testing. (b) Structure of the copolymer PMeld containing randomly distributed Meld-functional monomer units. (c) SEM images of PCL-PM1 and PCL-PM5 meshes from blends of PCL and PMeld.

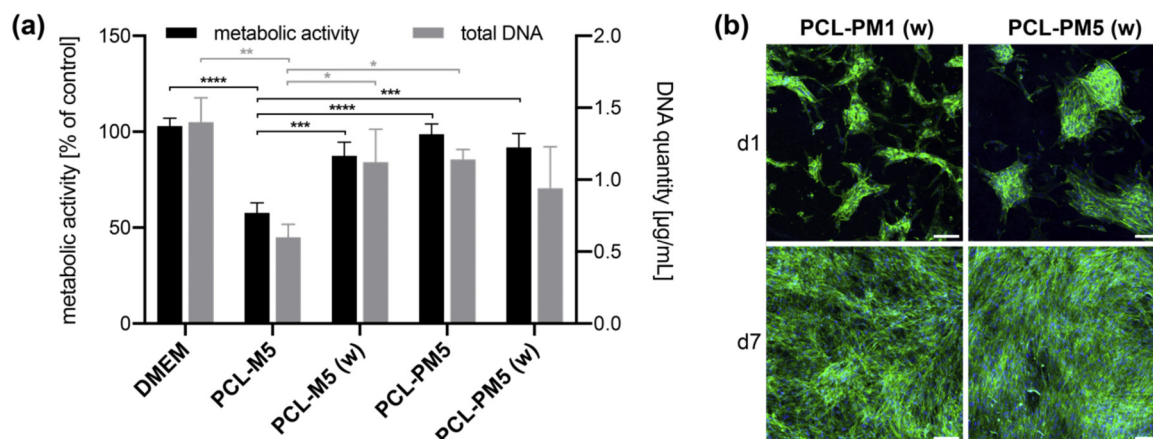


Fig. 5. (a) Cell metabolic activity and DNA quantification of hDF upon incubation with PCL-M5 and PCL-PM5 extracts from meshes with (w) or without prior washing with ethanol. Culture medium incubated for 24 h without mesh pieces was used as a control (DMEM). Values for metabolic activity were normalized to hDF cultured in a fresh culture medium. Data are expressed as mean \pm sd ($n = 3$). Statistical significance was set at * $p < 0.05$, ** $p < 0.01$, *** $p < 0.001$ and **** $p < 0.0001$. (b) hDF cultured for 1 and 7 days on washed PCL-PM1 and PCL-PM5 and stained for actin cytoskeleton (green) and nuclei (blue). Scale bar 100 μ m.

possibly due to the extremely low amount of Meld incorporated in these meshes. Notably, quantification of the total DNA content was similar to the observations of metabolic activity, showing a significantly lower DNA quantity only for unwashed PCL-M5 when compared to washed PCL-M5, washed/unwashed PCL-PM5 and DMEM control (Fig. 5a).

When culturing hDF directly on washed PCL-PM1 and PCL-PM5 meshes, the cells were able to attach to the meshes but formed clusters by day 1 (Fig. 5b). Notably, however, a confluent cell layer could be observed after 7 days of culture, indicative of good cell proliferation over the culture period. Taken together, these results demonstrate that PCL-PM1 and PCL-PM5 are cytocompatible in both indirect and direct contact (under the culture conditions specified here).

4. Conclusions

We presented a strategy to develop highly sensitive sensors for volatile amines based on FA and electrospun fibre meshes. The system is sensitive to several volatile amines, with the response depending on the amine properties. With the possibility of a two-factor calibration curve (based on the concentration of the analyte and exposure time) and of adjusting the sensitivity/response by changing the type and concentration of FA, the developed system could be used to detect a large number of amines over a wide detection range (ppb–ppm). With the optimization of the mesh structure and FA type, we decreased the detection limit to only 10 ppb of DEA. Additionally, the toxicity of activated FA which are precursors of DASA photochromes was assessed for the first time; by covalently attaching the FA to the polymer in the meshes, no toxicity against hDF was elicited in both direct and indirect cell contact tests. With further improvements, the developed system could find applications as colourimetric sensors for diagnosis in exhaled breath (to detect, among others, pneumonia or chronic kidney disease), for detecting illegal drugs (e.g., methamphetamines) or for workplace safety (to detect ammonia or toxic volatile amines). In the future, the meshes could be designed for integration into textiles while the detection system could be miniaturized and connected to a smartphone, making the whole setup a portable/wearable sensing platform for a quick, on-site assay of volatile amines.

Data availability statement

The raw/processed data required to reproduce these findings cannot be shared at this time due to technical or time limitations.

The raw/processed data required to reproduce these findings cannot be shared at this time as the data also forms part of an ongoing study.

CRediT authorship contribution statement

Sebastian Ulrich: Conceptualization, Data curation, Formal analysis, Investigation, Methodology, Writing - original draft. **Sara Oliveira Moura:** Conceptualization, Data curation, Formal analysis, Investigation, Methodology, Writing - original draft. **Yvonne Diaz:** Investigation, Methodology. **Michèle Clerc:** Investigation, Methodology, Data curation. **Anne Géraldine Guex:** Investigation, Methodology. **Javier Read de Alaniz:** Supervision, Funding acquisition. **Albino Martins:** Supervision. **Nuno M. Neves:** Supervision. **Markus Rottmar:** Conceptualization, Data curation, Formal analysis, Writing - original draft. **René M. Rossi:** Supervision, Funding acquisition. **Giuseppino Fortunato:** Supervision, Formal analysis, Project administration. **Luciano F. Boesel:** Project administration, Funding acquisition, Supervision, Writing - original draft.

Declaration of Competing Interest

The authors declare that they have no known competing financial interests or personal relationships that could have appeared to influence the work reported in this paper.

Acknowledgments

This work was supported by the Swiss National Science Foundation (SNSF) through the project 200021_172609. The authors thank Mr. Anjani Maurya for providing the Matlab code, Dr. Daniel Rentsch for the NMR measurements, and Yvonne Elbs-Glatz for supporting the cell culture experiments. The NMR hardware was partially granted by the SNSF (grant no. 206021_150638/1).

Appendix A. Supplementary data

Supplementary material related to this article can be found, in the online version, at doi:<https://doi.org/10.1016/j.snb.2020.128570>.

References

- [1] W.L. Gong, K.J. Sears, J.E. Alleman, E.R. Blatchley, Toxicity of model aliphatic amines and their chlorinated forms, *Environ. Toxicol. Chem.* 23 (2004) 239–244.
- [2] J.C. Eichhorst, M.L. Etter, N. Rousseaux, D.C. Lehotay, Drugs of abuse testing by tandem mass spectrometry: a rapid, simple method to replace immunoassays, *Clin. Biochem.* 42 (2009) 1531–1542.
- [3] S.J. Davies, P. Spanel, D. Smith, Breath analysis of ammonia, volatile organic compounds and deuterated water vapor in chronic kidney disease and during dialysis, *Bioanalysis* 6 (2014) 843–857.

- [4] B. Grabowska-Polanowska, M. Skowron, P. Miarka, A. Pietrzycka, I. Sliwka, The application of chromatographic breath analysis in the search of volatile biomarkers of chronic kidney disease and coexisting type 2 diabetes mellitus, *J. Chromatogr. B* 1060 (2017) 103–110.
- [5] A. Abd El Qader, D. Lieberman, Y. Shemer Avni, N. Svobodin, T. Lazarovitch, O. Sagi, Y. Zeiri, Volatile organic compounds generated by cultures of bacteria and viruses associated with respiratory infections, *Biomed. Chromatogr.* 29 (2015) 1783–1790.
- [6] H.N. Kim, Z. Guo, W. Zhu, J. Yoon, H. Tian, Recent progress on polymer-based fluorescent and colorimetric chemosensors, *Chem. Soc. Rev.* 40 (2011) 79–93.
- [7] X. Zhai, X. Zou, J. Shi, X. Huang, Z. Sun, Z. Li, Y. Sun, Y. Li, X. Wang, M. Holmes, Y. Gong, M. Povey, J. Xiao, Amine-responsive bilayer films with improved illumination stability and electrochemical writing property for visual monitoring of meat spoilage, *Sens. Actuators B* (2020) 302.
- [8] A. Domínguez-Aragón, J. Olmedo-Martínez, E. Zaragoza-Contreras, Colorimetric sensor based on a poly(ortho-phenylenediamine-co-aniline) copolymer for the monitoring of tilapia (*Oreochromis niloticus*) freshness, *Sens. Actuators B* 259 (2018) 170–176.
- [9] Q. Sui, P. Li, N.-N. Yang, T. Gong, R. Bu, E.-Q. Gao, Differentiable detection of volatile amines with a viologen-derived metal-organic material, *ACS Appl. Mater. Interfaces* 10 (2018) 11056–11062.
- [10] D. Zhao, L. Li, W. Niu, S. Chen, Highly conductive polythiophene films doped with chloroauric acid for dual-mode sensing of volatile organic amines and thiols, *Sens. Actuators B* 243 (2017) 380–387.
- [11] N. Jornet-Martínez, Y. Moliner-Martínez, R. Herráez-Hernández, C. Molins-Legua, J. Verdú-Andrés, P. Campíns-Falcó, Designing solid optical sensors for *in situ* passive discrimination of volatile amines based on a new one-step hydrophilic PDMS preparation, *Sens. Actuators B* 223 (2016) 333–342.
- [12] J.R. Askim, M. Mahmoudi, K.S. Suslick, Optical sensor arrays for chemical sensing: the optoelectronic nose, *Chem. Soc. Rev.* 42 (2013) 8649–8682.
- [13] Z. Li, J.R. Askim, K.S. Suslick, The optoelectronic nose: colorimetric and fluorometric sensor arrays, *Chem. Rev.* 119 (2019) 231–292.
- [14] S. Ulrich, J.R. Hemmer, Z.A. Page, N.D. Dolinski, O. Rifaie-Graham, N. Bruns, C.J. Hawker, L.F. Boesel, J. Read de Alaniz, Visible light-responsive DASA-polymer conjugates, *ACS Macro Lett.* 6 (2017) 738–742.
- [15] O. Rifaie-Graham, S. Ulrich, N. Galensowske, S. Balog, M. Chami, D. Rentsch, J. Hemmer, J. Read de Alaniz, L.F. Boesel, N. Bruns, Wavelength-selective light-responsive DASA-functionalized polymersome nanoreactors, *J. Am. Chem. Soc.* 140 (2018) 8027–8036.
- [16] S. Helmy, F.A. Leibfarth, S. Oh, J.E. Poelma, C.J. Hawker, J. Read de Alaniz, Photoswitching using visible light: a new class of organic photochromic molecules, *J. Am. Chem. Soc.* 136 (2014) 8169–8172.
- [17] S. Helmy, S. Oh, F.A. Leibfarth, C.J. Hawker, J. Read de Alaniz, Design and synthesis of donor-acceptor stenhouse adducts: a new visible light photoswitch derived from furfural, *J. Org. Chem.* 79 (2014) 11316–11329.
- [18] Y.J. Diaz, Z.A. Page, A.S. Knight, N.J. Treat, J.R. Hemmer, C.J. Hawker, J. Read de Alaniz, A versatile and highly selective colorimetric sensor for detection of amines, *Chem.-Eur. J.* (2017) 1–15.
- [19] Q. Chen, Y.J. Diaz, M.C. Hawker, M.R. Martinez, Z.A. Page, S. Xiao-An Zhang, C.J. Hawker, J. Read de Alaniz, Stable activated furan and donor-acceptor stenhouse adduct polymer conjugates as chemical and thermal sensors, *Macromolecules* 52 (2019) 4370–4375.
- [20] S. Agarwal, A. Greiner, J.H. Wendorff, Functional materials by electrospinning of polymers, *Prog. Polym. Sci.* 38 (2013) 963–991.
- [21] R.-E. Ghitecu, A.-M. Popa, A. Schipanski, C. Hirsch, G. Yazgan, V.I. Popa, R.M. Rossi, K. Maniura-Weber, G. Fortunato, Catechin loaded PLGA submicron-sized fibers reduce levels of reactive oxygen species induced by MWCNT *in vitro*, *Eur. J. Pharm. Biopharm.* 122 (2018) 78–86.
- [22] M.B. Bannwarth, A. Camerlo, S. Ulrich, G. Jakob, G. Fortunato, R.M. Rossi, L.F. Boesel, Ellipsoid-shaped superparamagnetic nanoclusters through emulsion electrospinning, *Chem. Commun.* 51 (2015) 3758–3761.
- [23] J. Geltmeyer, G. Vancouillie, I. Steyaert, B. Breyne, G. Cousins, K. Lava, R. Hoogenboom, K. De Buysser, K. De Clerck, Dye modification of nanofibrous silicon oxide membranes for colorimetric HCl and NH₃ sensing, *Adv. Funct. Mater.* 26 (2016) 5987–5996.
- [24] J. Wu, X. Lu, F. Shan, J. Guan, Q. Lu, Polydiacetylene-embedded supramolecular electrospun fibres for a colourimetric sensor of organic amine vapour, *RSC Adv.* 3 (2013) 22841–22844.
- [25] A. Akbarinejad, A. Ghoorchian, M. Kamalabadi, N. Alizadeh, Electrospun soluble conductive polypyrrole nanoparticles for fabrication of highly selective n-butylamine gas sensor, *Sens. Actuators B* 236 (2016) 99–108.
- [26] J. Yoon, Y.S. Jung, J.M. Kim, A combinatorial approach for colorimetric differentiation of organic solvents based on conjugated polymer-embedded electrospun fibers, *Adv. Funct. Mater.* 19 (2009) 209–214.
- [27] S. Jo, J. Kim, J. Noh, D. Kim, G. Jang, N. Lee, E. Lee, T.S. Lee, Conjugated polymer dots-on-electrospun fibers as a fluorescent nanofibrous sensor for nerve gas stimulant, *ACS Appl. Mater. Interfaces* 6 (2014) 22884–22893.
- [28] E. Schoolaert, R. Hoogenboom, K. De Clerck, Colorimetric nanofibers as optical sensors, *Adv. Funct. Mater.* 27 (2017) 1–26.
- [29] J.R. Hemmer, Z.A. Page, K.D. Clark, F. Stricker, N.D. Dolinski, C.J. Hawker, J. Read de Alaniz, Controlling dark equilibria and enhancing donor-acceptor stenhouse adduct photoswitching properties through carbon acid design, *J. Am. Chem. Soc.* 140 (2018) 10425–10429.
- [30] D. Kolbuk, S. Guimond-Lischer, P. Sajkiewicz, K. Maniura-Weber, G. Fortunato, The effect of selected electrospinning parameters on molecular structure of polycaprolactone nanofibers, *Int. J. Polym. Mater. Polym. Biomater.* 64 (2015) 365–377.
- [31] A. Tran-Ly, J. Ribera, F. Schwarze, M. Brunelli, G. Fortunato, Fungal melanin-based electrospun membranes for heavy metal detoxification of water, *Sustain. Mater. Technol.* 23 (2020) e00146.
- [32] M.A. Woodruff, D.W. Hutmacher, The return of a forgotten polymer-polycaprolactone in the 21st century, *Prog. Polym. Sci.* 35 (2010) 1217–1256.
- [33] G. Yazgan, R.I. Dmitriev, V. Tyagi, J. Jenkins, G.M. Rotaru, M. Rottmar, R.M. Rossi, C. Toncelli, D.B. Papkovsky, K. Maniura-Weber, G. Fortunato, Steering surface topographies of electrospun fibers: understanding the mechanisms, *Sci. Rep.* 7 (2017) 158–171.
- [34] M.M. Lerch, M. Di Donato, A.D. Laurent, M. Medved, A. Iagatti, L. Bussotti, A. Lapini, W.J. Buma, P. Foggi, W. Szymanski, B.L. Feringa, Solvent effects on the actinic step of donor-acceptor stenhouse adduct photoswitching, *Angew. Chem.* 130 (2018) 8195–8200.
- [35] M. Alves da Silva, A. Martins, A. Costa-Pinto, P. Costa, S. Faria, M. Gomes, R. Reis, N. Neves, Cartilage tissue engineering using electrospun PCL nanofiber meshes and MSCs, *Biomacromolecules* 11 (2010) 3228–3236.
- [36] A. Martins, E. Pinho, S. Faria, I. Pashkuleva, A. Marques, R. Reis, N. Neves, Surface modification of electrospun polycaprolactone nanofiber meshes by plasma treatment to enhance biological performance, *Small* 5 (2009) 1195–1206.
- [37] A. Morel, S. Domaschke, V. Urundil Kumar, D. Alexeev, A. Sadeghpour, S.N. Ramakrishna, S.J. Ferguson, R.M. Rossi, E. Mazza, A.E. Ehret, G. Fortunato, Correlating diameter, mechanical and structural properties of poly(L-lactide) fibres from needleless electrospinning, *Acta Biomater.* 81 (2018) 169–183.
- [38] J. Fernandes, P. Gentile, M. Martins, N. Neves, C. Miller, A. Crawford, R. Pires, P. Hattton, R. Reis, Reinforcement of poly-L-lactic acid electrospun membranes with strontium borosilicate bioactive glasses for bone tissue engineering, *Acta Biomater.* 44 (2016) 168–177.
- [39] S. Devic, J. Seuntjens, E. Sham, E.B. Podgorsak, C.R. Schmidlein, A.S. Kirov, C.G. Soares, Precise radiochromic film dosimetry using a flat-bed document scanner, *Med. Phys.* 32 (2005) 2245–2253.
- [40] S.C. Wong, A. Baji, S. Leng, Effect of fiber diameter on tensile properties of electrospun poly(ϵ -caprolactone), *Polymer* 49 (2008) 4713–4722.
- [41] A. Morel, S.C. Oberle, S. Ulrich, G. Yazgan, F. Spano, S.J. Ferguson, G. Fortunato, R.M. Rossi, Revealing non-crystalline polymer superstructures within electrospun fibers through solvent-induced phase rearrangements, *Nanoscale* 11 (2019) 16788–16800.
- [42] H. Wolrath, H. Borén, A. Hallén, U. Forsum, Trimethylamine content in vaginal secretion and its relation to bacterial vaginosis, *APMIS* 110 (2002) 819–824.

Dr. Sebastian Ulrich is currently working as a scientist in chemical process development for Sigma-Aldrich, subsidiary of the Merck Group/EMD. He holds a PhD in chemistry from the Adolphe Merkle Institute of the University of Fribourg (Switzerland) and conducted his PhD and postdoctoral research at Empa, the Swiss Federal Laboratories for Materials Science and Technology.

Dr. Luciano F. Boesel is currently Group Leader at Empa, the Swiss Federal Laboratories for Materials Science and Technology, in Switzerland. He has a PhD in Materials Science and Technology (Biomaterials) from the Univ. of Minho (Portugal). Before joining Empa in 2010, he was a Marie Curie Research Fellow at the Institute of Science and Technology of Polymers (CSIC, Spain) and an Alexander von Humboldt Fellow at the Max-Planck Institute for Polymer Research (Germany). His main focus of activities are the development of non-invasive sensors (physical, chemical, bio) for monitoring body parameters, and the development of drug delivery systems based on light-responsive materials.